

Immobilization of nanocarriers within a porous chitosan scaffold for the sustained delivery of growth factors in bone tissue engineering applications

De Witte, Tinke Marie; Wagner, Angela M.; Fratila-Apachitei, Lidy E.; Zadpoor, Amir A.; Peppas, Nicholas A.

DOI

[10.1002/jbm.a.36887](https://doi.org/10.1002/jbm.a.36887)

Publication date

2020

Document Version

Final published version

Published in

Journal of Biomedical Materials Research - Part A

Citation (APA)

De Witte, T. M., Wagner, A. M., Fratila-Apachitei, L. E., Zadpoor, A. A., & Peppas, N. A. (2020). Immobilization of nanocarriers within a porous chitosan scaffold for the sustained delivery of growth factors in bone tissue engineering applications. *Journal of Biomedical Materials Research - Part A*, 108(5), 1122-1135. <https://doi.org/10.1002/jbm.a.36887>

Important note

To cite this publication, please use the final published version (if applicable).
Please check the document version above.

Copyright

Other than for strictly personal use, it is not permitted to download, forward or distribute the text or part of it, without the consent of the author(s) and/or copyright holder(s), unless the work is under an open content license such as Creative Commons.

Takedown policy

Please contact us and provide details if you believe this document breaches copyrights.
We will remove access to the work immediately and investigate your claim.


Green Open Access added to TU Delft Institutional Repository

'You share, we take care!' - Taverne project

<https://www.openaccess.nl/en/you-share-we-take-care>

Otherwise as indicated in the copyright section: the publisher is the copyright holder of this work and the author uses the Dutch legislation to make this work public.

Immobilization of nanocarriers within a porous chitosan scaffold for the sustained delivery of growth factors in bone tissue engineering applications

Tinke-Marie De Witte^{1,2}  | Angela M. Wagner^{3,4} | Lidy E. Fratila-Apachitei² | Amir A. Zadpoor² | Nicholas A. Peppas^{1,3,4,5,6}

¹Department of Biomedical Engineering, The University of Texas at Austin, Austin, Texas

²Department of Biomechanical Engineering, Delft University of Technology (TU Delft), Delft, Netherlands

³McKetta Department of Chemical Engineering, The University of Texas at Austin, Austin, Texas

⁴Institute for Biomaterials, Drug Delivery, and Regenerative Medicine, The University of Texas at Austin, Austin, Texas

⁵Department of Pediatrics, and Department of Surgery and Perioperative Care, Dell Medical School, The University of Texas at Austin, Austin, Texas

⁶Division of Molecular Pharmaceutics and Drug Delivery, College of Pharmacy, The University of Texas at Austin, Austin, Texas

Correspondence

Nicholas A. Peppas, Department of Biomedical Engineering, The University of Texas at Austin, BME 3.503C, 107 W. Dean Keeton, BME Building, 1 University Station, C0800, Austin, TX 78712.

Email: peppas@che.utexas.edu

Funding information

National Institutes of Health, Grant/Award Number: R01-EB022025

Abstract

To guide the natural bone regeneration process, bone tissue engineering strategies rely on the development of a scaffold architecture that mimics the extracellular matrix and incorporates important extracellular signaling molecules, which promote fracture healing and bone formation pathways. Incorporation of growth factors into particles embedded within the scaffold can offer both protection of protein bioactivity and a sustained release profile. In this work, a novel method to immobilize carrier nanoparticles within scaffold pores is proposed. A biodegradable, osteoconductive, porous chitosan scaffold was fabricated via the “freeze-drying method,” leading to scaffolds with a storage modulus of 8.5 kPa and 300 μm pores, in line with existing bone scaffold properties. Next, poly(methyl methacrylate-co-methacrylic acid) nanoparticles were synthesized and immobilized to the scaffold via carbodiimide-crosslinker chemistry. A fluorescent imaging study confirmed that the conventional methods of protein and nanocarrier incorporation into scaffolds can lead to over 60% diffusion out of the scaffold within the first 5 min of implantation, and total disappearance within 4 weeks. The novel method of nanocarrier immobilization to the scaffold backbone via carbodiimide-crosslinker chemistry allows full retention of particles for up to 4 weeks within the scaffold bulk, with no negative effects on the viability and proliferation of human umbilical vein endothelial cells.

KEYWORDS

3D porous scaffold, bone regeneration, chitosan scaffold, growth factor delivery, sustained release

1 | INTRODUCTION

Bone-related disorders continue to have a significant effect on people, especially in areas affected by an ageing population (Amini, Lauren, & Nukavarapu, 2012). Recent market analyses suggest that annually over 20 million people worldwide are affected by a lack of bone tissue due to injury or disease, resulting in over 5 million orthopedic procedures annually (Habibovic, 2017). For large bony defects that are not capable of self-repair and can occur as a result of traumatic

fracture, tumor resection, or endoprosthetic loosening, the current gold standard treatment options include bone allografts and autografts (Fröhlich et al., 2008). Bone autografts rely on the harvesting of bone from another part of the patient's body, such as the iliac crest or parts of the tibia (Myeroff & Archdeacon, 2011) and present the advantage of being osteoconductive, angiogenic, and immunocompatible. However, bone autografts can result in a variety of complications including donor site morbidity, infection, pain, and fracture at the donation site (Calori et al., 2014; Dimitriou,

Mataliotakis, Angoules, Kanakaris, & Giannoudis, 2011). Bone allografts, consisting of bone harvested from a donor corpse, eliminate donor site-related complications, but present additional challenges, such as the risk of negative immune response and disease transmission. In response to these limitations of the current gold standard treatment options, the field of bone tissue engineering has emerged, as it presents a promising solution to these limitations.

Bone tissue engineering relies on the use of biodegradable scaffolds, which mimic the extracellular matrix and guide the natural bone formation process (Bose, Roy, & Bandyopadhyay, 2012; Oryan, Alidadi, Moshiri, & Maffulli, 2014). Successful bone tissue engineering scaffolds present an interconnected porosity, typically with a mean pore size around 300 μm (Saravanan, Leena, & Selvamurugan, 2016) as well as mechanical properties, such as compressive strengths similar to that of the native bone. While metals and ceramics have been explored as scaffold materials, natural polymers including chitosan and their composites have been of particular interest in the development of bone scaffolds due to their inherent chemical biocompatibility and proven osteoconductivity (Balagangadharan, Dhivya, & Selvamurugan, 2017).

In addition, recent reports indicate the importance of incorporating signaling molecules into bone tissue engineering strategies in order to enhance the recruitment of cells, osteogenic differentiation, and angiogenesis, phases which are crucial to bone tissue regeneration. A class of growth factors qualified as bone morphogenetic proteins (BMPs) and the members of the TGF- β superfamily (Chen, Zhao, & Mundy, 2004) represent some particularly interesting candidates for that purpose. Specifically, BMP-2 and BMP-7 have been identified as playing an important role in osteogenic differentiation. In addition, these factors have been incorporated in FDA-approved commercial systems for spinal fusions (El Bialy, Jiskoot, & Reza Nejadnik, 2017).

Three categories of techniques have been widely explored to deliver growth factors in a sustained and controlled way (De Witte, Fratila-Apachitei, Zadpoor, & Peppas, 2018). Among those, the physical entrapment or adsorption of growth factors to the scaffold has been successfully used for burst release of growth factors. However, this method does not allow for a sustained delivery of the payload, due to its rapid diffusion out of the scaffold (Vo, Kasper, & Mikos, 2012). The second category of techniques that are based on the covalent binding of proteins to scaffolds lead to constant, sustained protein release profiles. These techniques fail to prevent the rapid degradation and loss of bioactivity of the protein (Di Luca et al., 2017). Finally, the incorporation of proteins into particles has shown great promise for controlled release and is able to both protect the protein and provide a delivery profile consisting of an initial burst release followed by a short, sustained release (Bessa et al., 2010; Subbiah et al., 2015). Unfortunately, as with the method of protein adsorption to the scaffold, this method does not limit the ability of particles to diffuse through the large scaffold pores and be released from the targeted site.

Here, we propose a novel method to immobilize carrier nanoparticles within scaffold pores, thereby ensuring the sustained retention of proteins. Chitosan, a chemically biocompatible and biodegradable natural polymer with osteoconductive properties was used to fabricate a highly porous scaffold. Poly(methyl methacrylate-co-methacrylic acid) (P[MMA-co-MAA]) nanoparticles were then synthesized and immobilized within the scaffold pores using carbodiimide-crosslinker chemistry (Figure 1). Ultimately, this system seeks to address some of the key challenges in the development of bone tissue engineering scaffolds and aims to present a versatile and robust approach for the controlled delivery of growth factors.

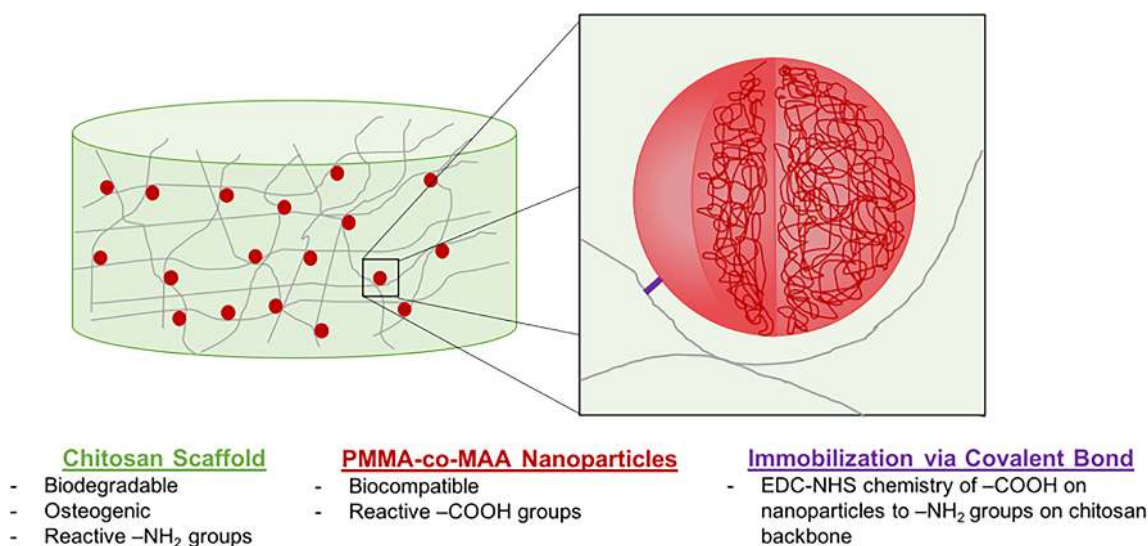


FIGURE 1 Design of a two-phase nanoparticle-scaffold system relying on the immobilization of P(MMA-co-MAA) nanoparticles to a chitosan scaffold backbone for the sustained delivery of growth factors in bone tissue engineering applications

2 | METHODS

2.1 | Materials

Chitosan powder (high molecular weight, weight-average molar mass: 310–375 kDa, 85% deacetylated, 200–800 cP, Catalog 448877) was obtained from Sigma-Aldrich (Sigma-Aldrich Corporation, St Louis, MO). Acetic acid (glacial, Certified ACS) and sodium carbonate (anhydrous, Powder) were obtained from Thermo Fisher Scientific (Thermo Fisher Scientific, Waltham, MA). Dulbecco's phosphate-buffered saline (DPBS) was obtained from Thermo Fisher Scientific.

Methyl methacrylate (MMA, 99%, Catalog M55909) and methacrylic acid (MAA, 99%, Catalog 155721) were obtained from Sigma-Aldrich. Polyethylene glycol dimethacrylate with PEG molecular weight 600 (PEGDMA 600, Catalog 02364) was obtained from Polysciences, Inc (Polysciences, Inc., Warrington, PA). The initiator Irgacure 2959 was obtained from Ciba (Ciba Inc., Basel, Switzerland), while the surfactants Brij 30 and MyTab were obtained from Thermo Fisher Scientific and Sigma-Aldrich, respectively.

Trypsin from bovine pancreas (powder, Catalog T9201) was obtained from Sigma-Aldrich. DAPI (4',6-diamidino-2-phenylindole, dihydrochloride, Catalog D1306) and FITC (5/6-fluorescein isothiocyanate, Catalog 46,425) were obtained from Thermo Fisher Scientific, and tetramethylrhodamine (TAMRA) cadaverine (Catalog 92001) was obtained from Biotium (Biotium Inc., Fremont, CA.)

HUV-EC-C (HUVEC; ATCC CRL-1730) and F-12K Medium (Kaighn's Modification of Ham's F-12 Medium, ATCC 30-2004) were obtained from ATCC (ATCC, Manassas, VA). Heparin sodium (Catalog AC411210010) and fetal bovine serum (Corning, Catalog 35010CV) were obtained from Thermo Fisher Scientific. Endothelial cell growth supplement from bovine neural tissue (ECGS, Catalog E2759) was obtained from Sigma-Aldrich.

2.2 | Scaffold fabrication

In typical experiments, chitosan scaffolds were prepared by dissolving 1, 2, 3, or 4 wt% chitosan powder (Figure 2) in 2 vol% (0.34 M) acetic acid. The solutions were placed on a disk rotator and left for 10–12 hr to allow the chitosan to dissolve. A sample of 2.0 ml of the solution was then cast into each well of a 24-well polystyrene plate using a syringe. The plates were then placed in a 37°C incubator overnight. Following incubation, the specimens were collected and immersed in 1 M sodium carbonate solution in order to neutralize acetate

functional groups. Subsequently, 0.8 ml of sodium carbonate solution was added to each well and the plates were placed on a plate shaker for 2 hr. In order to avoid an excessive amount of sodium acetate salts, excess liquid was removed from the wells. The plates were then frozen at -80°C for 24 hr. After freezing, the samples were lyophilized in a freeze drier (FreeZone Cascade Benchtop Freeze Dry System, Labconco, Kansas City, MO) under vacuum at -105°C for 48 hr.

2.3 | Scaffold characterization

2.3.1 | Scanning electron microscope imaging

Scanning electron microscope (SEM) images were obtained in order to determine the microscopic structure of the lyophilized chitosan scaffolds with varying wt% (1, 2, 3, and 4 wt%). The freeze-dried chitosan scaffold samples were sputter-coated with 12 nm of platinum/palladium (Pt/Pd) at 20 mA and were imaged by SEM (Supra 40VP SEM, Zeiss, Oberkochen, Germany).

2.3.2 | Dynamic mechanical properties

The storage, G' , and loss, G'' , moduli of the specimens in the hydrated state were determined using a rheometer (Discovery Hybrid Rheometer, TA Instruments, New Castle, DE). Chitosan scaffolds were hydrated in 2.0 ml of 1× DPBS for 1 hr at room temperature. In order to remove the residual sodium acetate salts, the DPBS was replaced three times. With each rinse, the scaffolds were incubated with fresh DPBS for 1 hr at room temperature and with gentle agitation. A rheometer immersion ring accessory (Peltier Plater Immersion Ring, TA Instruments, New Castle, DE) was used in order to submerge the chitosan scaffolds in 1× DPBS and maintain constant levels of hydration during testing.

The linear elastic range of the materials was determined by performing a frequency sweep from 0.01 to 10 Hz at 1% strain. All samples showed purely viscous behavior at frequencies above 0.6 Hz. All subsequent tests were performed at 1% strain from 0.01 to 0.6 Hz. The mechanical properties of the scaffolds with increasing wt% chitosan (1, 2, 3, or 4 wt%; $n = 6$ per formulation) were compared. Average values and standard deviations were calculated from the measured values at 0.1 Hz. The measured values of the storage modulus correspond to the stored energy and describe the elastic behavior of the material while the loss modulus corresponds to the energy

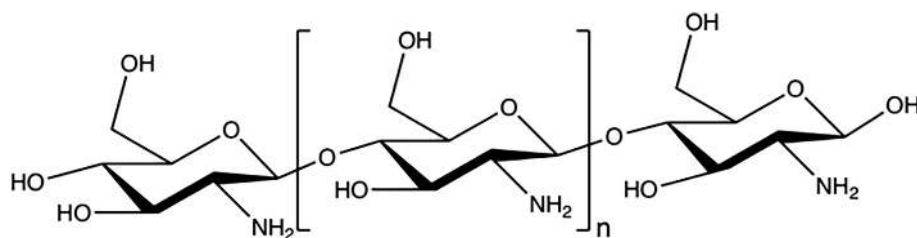


FIGURE 2 The chemical structure of chitosan

dissipation due to the viscous behavior of the material. The ratio of the loss to storage modulus, $\tan(\delta)$, indicates the relative elastic behavior of the tested material, with values below 1 indicating solid- or gel-like behavior.

The obtained values of $\tan(\delta)$ were analyzed using a one-way ANOVA test ($\alpha = 0.05$) with post hoc Tukey HSD Test ($\alpha = 0.05$). Statistically significant differences are noted as $p < 0.01$ (**) or, in case of no statistical significance, "ns".

2.4 | Synthesis of nanoparticles

P(MMA-co-MAA) nanoparticles were synthesized using the reproducible method of UV-initiated, aqueous emulsion free radical polymerization (Fisher & Peppas, 2009). Aqueous emulsion polymerization requires the use of hydrophobic monomers, which partition into the oil droplet phase. In addition, particle size is controllable by varying the relative amounts of surfactants, initiator, and crosslinking density.

To synthesize the P(MMA-co-MAA) nanoparticles, the pre-polymerization mixture was prepared by combining 95 mol% methyl methacrylate, 4 mol% methacrylic acid and 1 mol% poly(ethylene glycol) dimethacrylate (PEGDMA) with average PEG MW = 600 in a round-bottom flask. An aqueous solution was formed by adding 25.0 ml of deionized water. In order to form an emulsion, Brij 30, a nonionic surfactant, and myristyl trimethyl ammonium bromide (MyTAB), a cationic surfactant, were added to the aqueous solution at the concentrations of 4 mg/ml and 1.16 mg/ml, respectively. Finally, the free radical initiator Irgacure 2925 was added at a ratio of 0.5 wt %. The chemical structures of the main chemical compounds involved in the emulsion polymerization are shown in Figure 3.

The reagents were then mixed by ultrasound for 20 min in order to form an oil-in-water emulsion, which was then purged with nitrogen in order to eliminate free radical scavengers. Subsequently, the emulsion was placed under a UV point source with an intensity of 140 mW/cm² for 2.5 hr (BlueWave 200 Spot Lamp System, Dymax Corporation, Torrington, CT). The synthesized particles were purified by diluting them at 1:1 in a 6.0 N HCl solution, followed by a dilution at 1:10 in 1× DPBS. The diluted particles were then centrifuged at 4,000g for 5 min so as to form a pellet. The supernatant was then removed, and the nanoparticle pellets were resuspended in 1× DPBS and adjusted to a pH of 7. Finally, the particle solutions were lyophilized under vacuum at -105°C for 48 hr. The nanoparticle synthesis method is summarized in Figure 4.

After purification, the hydrodynamic diameter of the nanoparticles was determined by dynamic light scattering (Zetasizer Nano, Malvern) using 5× diluted nanoparticle samples in 1× DPBS ($n = 3$ per formulation). In addition, the zeta potential of the nanoparticles was measured as a function of pH in order to determine the net charges present on the particles.

2.5 | Particle immobilization to the scaffold backbone

A fluorescent imaging study was carried out in order to compare three distinct systems over time (Figure 5) including the free protein adsorbed to the scaffold (System I), the free nanoparticles simply entrapped in the scaffold (System II), and the nanoparticles immobilized to the scaffold by carbodiimide-crosslinker chemistry between the carboxylic acids on the surface of the nanoparticles and the primary amines on the chitosan scaffold backbone (System III).

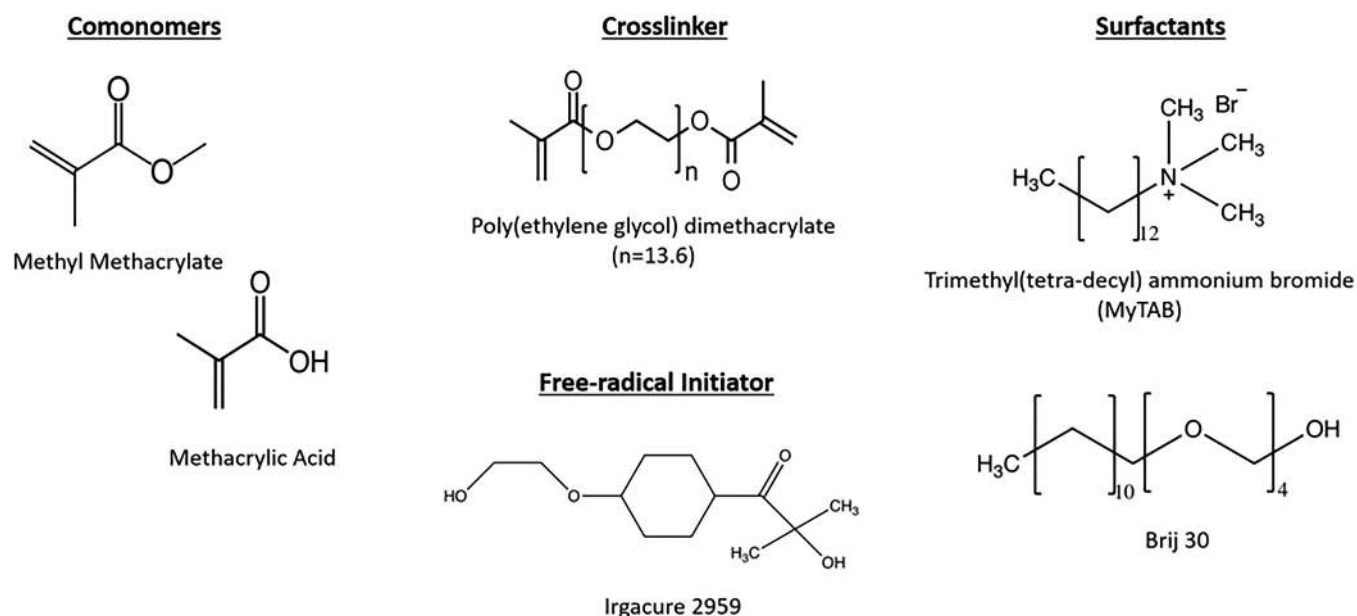


FIGURE 3 The chemical structures of the comonomers, crosslinker, surfactants, and free-radical initiator used for the fabrication of P(MMA-co-MAA) nanoparticles

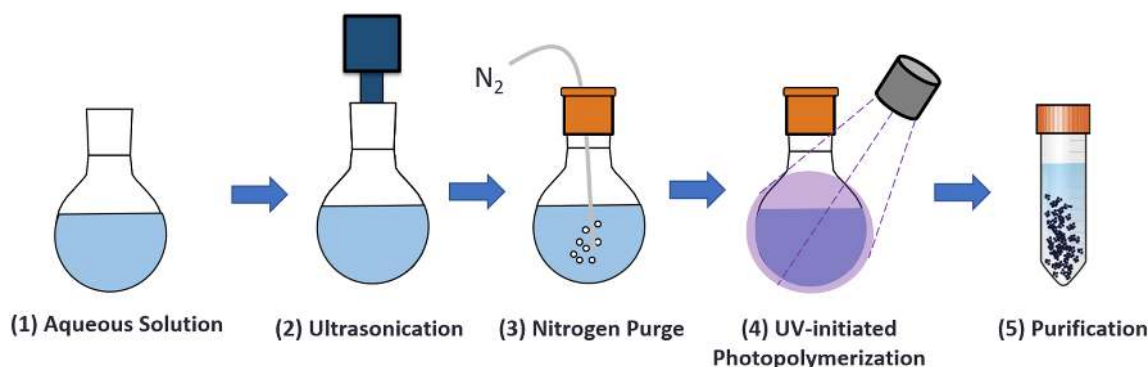


FIGURE 4 The main steps in the one-pot UV-initiated emulsion polymerization of polymeric nanoparticles: (1) preparation of the prepolymerization solution; (2) ultrasonication for 20 min to form an oil-in-water emulsion; (3) nitrogen purge to eliminate free radical scavengers; (4) reaction for 2.5 hr; (5) purification by precipitation in acid

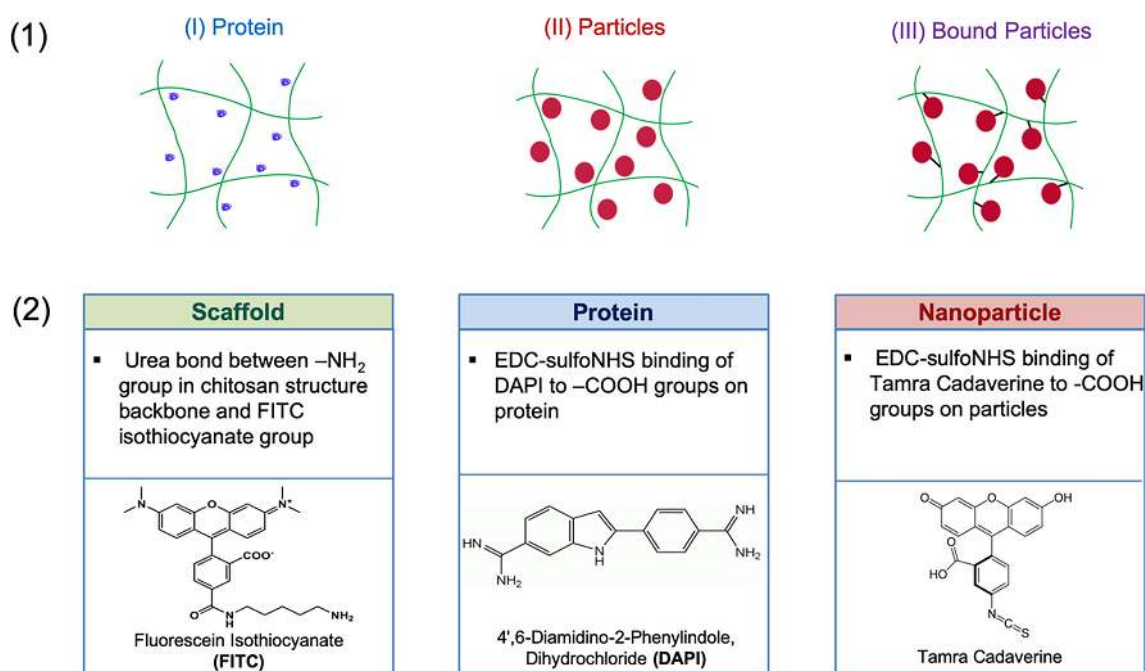


FIGURE 5 (a) The representative diagram of three distinct scaffold systems: (System I) free protein adsorbed to the scaffold, (System II) free nanoparticles simply entrapped in the scaffold, and (System III) nanoparticles immobilized to the scaffold by carbodiimide-crosslinker chemistry. (b) Fluorescent tagging agents used for scaffold, protein, and nanoparticles

2.5.1 | Fluorescent labeling of system components

Each component of the system was first labeled with a distinct fluorescent dye (Figure 5b). The chitosan scaffolds were labeled using fluorescein isothiocyanate (FITC; green fluorescent dye) by forming a urea bond with the primary amine groups on the scaffold backbone. A 10 mg/ml solution of FITC in DMF was added to each scaffold at a ratio of 0.067 v/v% FITC to scaffold. Trypsin was labeled using 4',6-diamidino-2-phenylindole, dihydrochloride (DAPI; blue fluorescent dye). A 10 mg/ml solution of DAPI in deionized water was added to a solution of trypsin at a ratio of 0.22 mg DAPI/mg trypsin. Finally, P(MMA-co-MAA) nanoparticles were labeled using TAMRA cadaverine (red fluorescent dye). A 70 mg/ml solution of TAMRA cadaverine

in ethanol was added to a 10 mg/ml solution of the nanoparticles at a ratio of 5 mg TAMRA cadaverine/mg nanoparticles.

2.5.2 | Preparation of distinct scaffold systems

After fluorescent labeling, the three distinct systems were prepared. For System I, DAPI-labeled trypsin was loaded into the scaffolds by incubating the scaffold in a protein solution similar to the adsorption loading methods existing in the literature (Figure 5a). The protein was loaded at a concentration of 1 mg/ml of scaffold, concentrations which are commonly used for similar systems in the literature as well as commercially available systems. For System II, the nanoparticles

were loaded into the scaffold at a concentration of 100 μl nanoparticle solution/ml scaffold using a 2 mg/ml stock solution of P(MMA-co-MAA) nanoparticles. Finally, for System III, carbodiimide-crosslinker chemistry was used to bind the carboxylic groups on the nanoparticles to the primary amines of the chitosan backbone, and nanoparticles were loaded at the same ratio as in System II. This was done by first activating the TAMRA cadaverine-labeled nanoparticles using 1-ethyl-3-(3-dimethylaminopropyl) carbodiimide hydrochloride (EDC) and sulfo-N-hydroxysulfosuccinimide (NHS). A 2 mg/ml solution of the nanoparticles was prepared by combining stock solutions of EDC in ethanol, sulfo-NHS in ethanol, and the labeled nanoparticles in 1 \times DPBS at a mass ratio of 0.4:1.1:0.5. The solution was adjusted to pH 6 and maintained at room temperature for 15 min to allow for the activation reaction with EDC and sulfo-NHS. The solution was then adjusted to pH 7.2 and 200 μl was added to each scaffold. The scaffolds were maintained at pH 7.2 and at room temperature to allow for the reaction of sulfo-NHS activated nanoparticles with the primary amines on the scaffold backbone. After 10 hr, the scaffolds were washed with fresh 1 \times DPBS and stored at room temperature.

2.5.3 | Fluorescent imaging of scaffold–nanoparticle and scaffold–protein systems

The labeled systems were then incubated in DPBS for up to 4 weeks. In order to mimic the fluid flow in the body, washes were performed every 5 min for the first 30 min of incubation followed by every 30 min for the following 3 hr. Fluorescent images were obtained using a manual inverted microscope (IX73, Olympus) using the phase contract to visualize the naked scaffold, DAPI filter to visualize the labeled protein, GFP filter to visualize the labeled scaffold backbone, and RFP filter to visualize the labeled nanoparticles. Images were obtained immediately after loading, after 30 min, 72 hr, and after 4 weeks in order to determine the relative change over time in the protein content for System I and in the particles for Systems II and III.

2.5.4 | Quantitative analysis of protein and nanoparticle diffusion from scaffold

Washes were performed every 5 min for the first 30 min, after 24 hr, 72 hr, and 4 weeks on the scaffolds containing fluorescently labeled protein and nanoparticles. After each wash, the supernatants were plated on a 96-well plate. For the DAPI-labeled protein, fluorescence was analyzed at an excitation wavelength of 358 nm and an emission wavelength of 461 nm. For the TAMRA cadaverine-labeled nanoparticles, fluorescence was analyzed at an excitation wavelength of 552 nm and an emission wavelength of 578 nm. The obtained fluorescence values were fitted to the calibration curves of the labeled components in order to obtain values of the concentration of the fluorescently labeled components in the supernatant.

2.6 | In vitro studies: Cell viability and proliferation

2.6.1 | Cell culture

The cytocompatibility of the two-phase scaffold–nanoparticle system was analyzed using nonimmortalized human umbilical vein endothelial cells (HUVEC) obtained from ATCC. The cells were propagated for two passages using an F-12K medium with 0.1 mg/ml heparin, 1 v/v% endothelial cell growth supplement, and 10 v/v% fetal bovine serum.

Cell culture treated 96-well plates were coated with 50 μl of a 1:100 fibronectin solution in 1 \times DPBS and incubated at room temperature for 1 hr. The fibronectin solution was then removed from the plate and the wells were rinsed with DPBS.

Two systems were evaluated for cytotoxicity: (i) 2 wt% chitosan scaffolds, and (ii) covalently bound p(MMA-co-MAA) nanoparticles to 2 wt% chitosan scaffolds. For system (ii), 2 wt% chitosan scaffolds with covalently bound particles at a concentration of 0.2 mg/ml nanoparticle to scaffold were used.

The scaffolds were sectioned into 3 mg pieces, sterilized by UV exposure, and incubated in HUVEC media overnight. The scaffolds were placed in the wells prior to cell seeding in order to allow for improved contact between the cells and scaffold. HUVEC cells were then seeded at 3,000 cells per well and allowed to incubate at room temperature for 1 hr. In addition to the scaffold systems, cells were incubated in HUVEC media (positive control) and with both triton and SDS (negative lysis controls).

All samples were then incubated for 24 and 48 hr in a humidified environment at 37°C and 5% CO₂. For all conditions and for each time point, $n = 12$.

2.6.2 | MTS cell proliferation assay

Cell proliferation in the presence of the system components after 24 and 48 hr was determined using an MTS cellular proliferation assay and used as an indicator of cell health. The CellTiter 96 AQueous One Solution Cell Proliferation Assay (Promega Corporation, Madison, WI) was used per manufacturer's instructions, and the resulting absorbances of the plate at 490 and 690 nm were obtained. The relative cellular proliferation was calculated by first subtracting the background absorbance at 690 nm from the absorbance at 490 nm. Subsequently, the obtained values were normalized to the average absorbance of the positive and negative controls (HUVEC cells in the HUVEC media and lysis control, respectively) in order to obtain the average cell proliferation for each condition ($n = 6$ per condition.)

2.6.3 | LDH membrane integrity assay

Cell membrane integrity in the presence of the system components after 24 and 48 hr was determined using a lactose dehydrogenase (LDH) membrane integrity assay as an indicator of cell health. The Promega CytoTox-ONE Homogeneous Membrane Integrity Assay

(Promega Corporation, Madison, WI) was used per manufacturer's instructions. The resulting fluorescence of the samples was measured at an excitation of 560 nm and an emission of 590 nm. The background fluorescence values as a result of the cell culture media were first subtracted from the obtained fluorescence values. These were then normalized to the average maximum LDH release (lysis control) and minimum LDH release (media control) in order to obtain the average cell viability for each condition ($n = 6$ per condition.)

3 | RESULTS

3.1 | Scaffold properties

Chitosan scaffolds with varying wt% of chitosan were prepared in order to optimize the fabrication of scaffolds to be used in the

proposed system. An increase in wt% of chitosan had a slight effect on the storage and loss moduli of the materials, increasing from 6,900 to 9,100 Pa and decreasing from 628 to 551 Pa, respectively (Figure 7). However, an increase in chitosan wt% resulted in a noticeable increase in the viscosity of the chitosan solution during experimental handling. Because the scaffold fabrication process required the casting of chitosan solution into molds, increased viscosity can result in a loss of material and the introduction of large air bubbles. It was, therefore, found that a 2 wt% formulation provided the best trade-off between higher mechanical properties and ease of handling.

SEM images indicated that a highly porous network was formed within the scaffold bulk (Figure 6). A hierarchical structure was observed, with smaller pores of around 300 μm in diameter as well as macropores (Figure 6a). In addition, an anisotropic structure was observed, with pores oriented orthogonally to the image plane (Figure 6b). As noted experimentally, this direction coincided with the

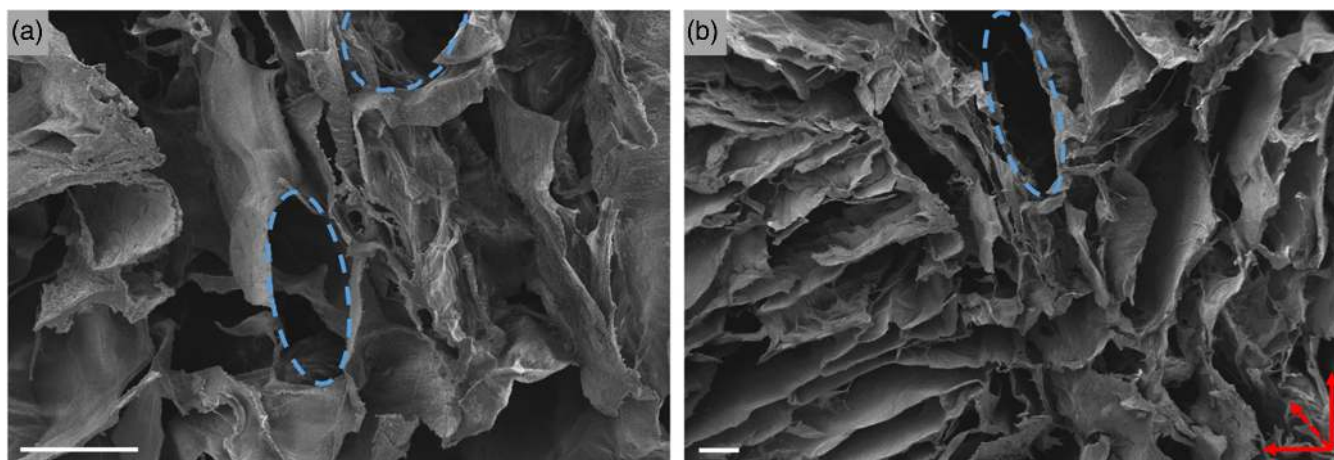


FIGURE 6 The SEM images of 2 wt% chitosan scaffolds at (a) 300 \times magnification and (b) 100 \times magnification. Scale bars = 200 μm . Blue dotted lines indicate visible pore structures while red dotted arrow indicates pore direction

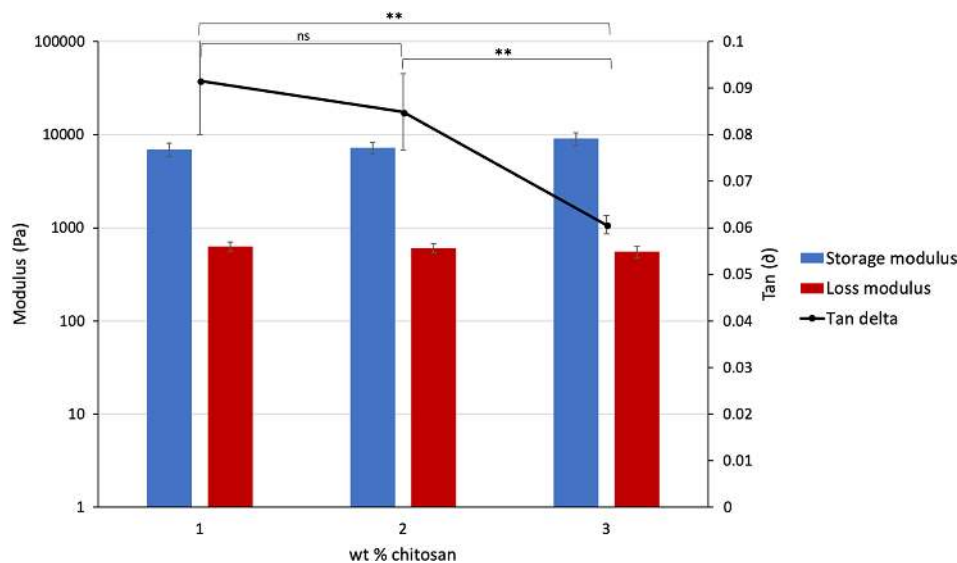


FIGURE 7 The dynamic mechanical properties of chitosan scaffolds with increasing wt% chitosan formulation. ns indicates difference not significant; ** indicates significance with $p < .01$

direction of the solvent sublimation during the freeze-drying process as well as the direction of loading during the dynamic mechanical tests.

The rheology data obtained for the chitosan scaffolds indicated that the 2 wt% chitosan scaffolds present a storage modulus (G') of around 8,300 Pa and a loss modulus (G'') of 606 Pa with a $\tan(\delta)$ of

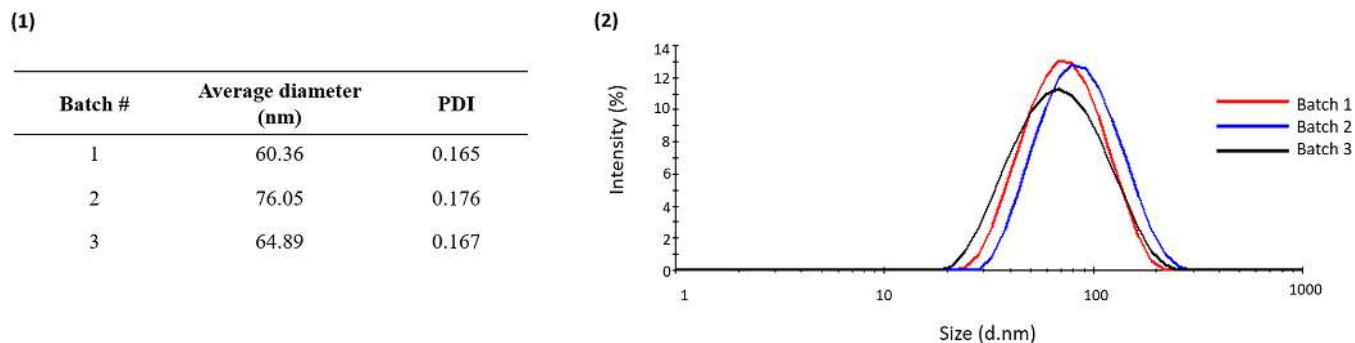


FIGURE 8 The dynamic light scattering results of nanoparticles synthesized using one-pot UV-initiated emulsion polymerization. (a) The batch-to-batch variability of the average hydrodynamic diameter of the nanoparticles and respective polydispersity indices. (b) The plot of the intensity distribution of hydrodynamic diameters for different batches

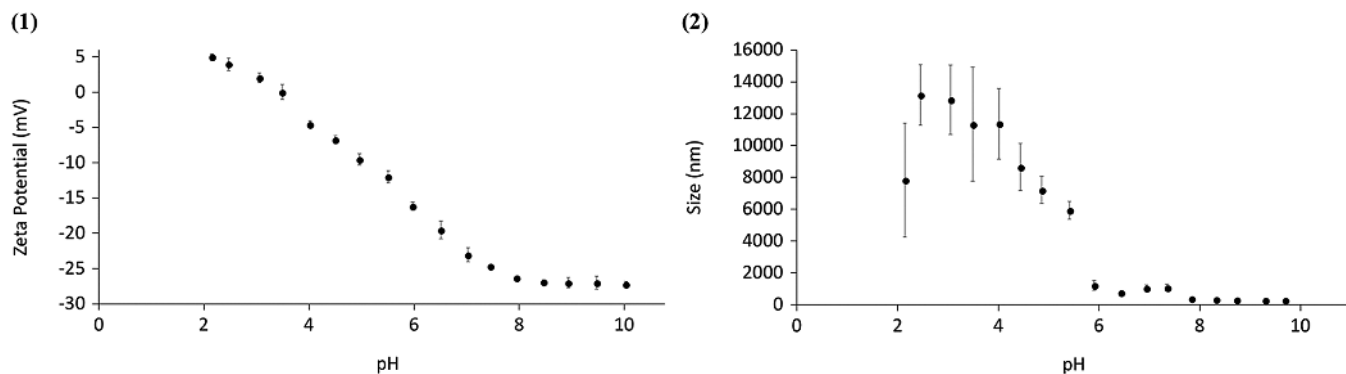


FIGURE 9 (a) Zeta potential and (b) particle size as a function of pH for P(MMA-co-MAA) nanoparticles

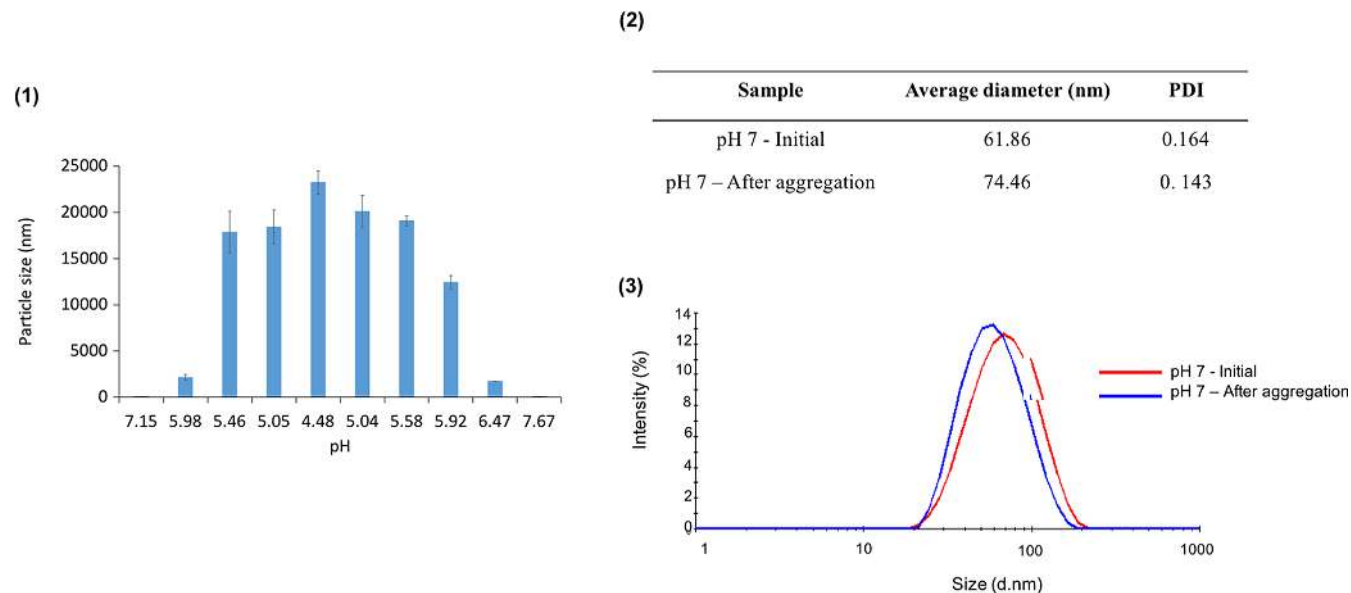


FIGURE 10 (a) The plot of recorded particle size in nm as a function of pH where pH is decreased from above pH 7 to pH 4.5 then increased again to above pH 7, (b) the average diameter and PDI of the nanoparticles before and after reversible aggregation, and (c) the intensity plots of the particle size before and after reversible aggregation

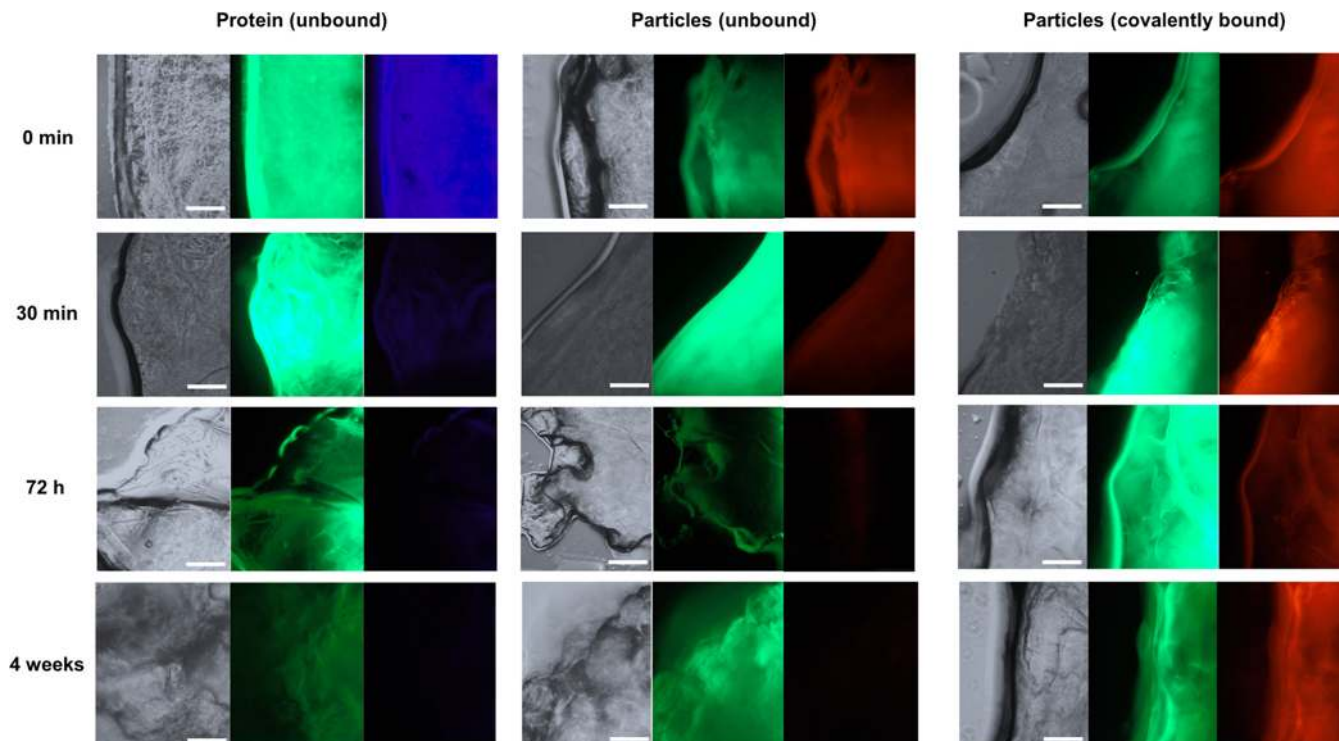


FIGURE 11 The fluorescent images of FITC-labeled chitosan scaffolds (green) incorporated with unbound DAPI-labeled trypsin (blue, Column 1), unbound Tamra cadaverine-labeled nanoparticles (red, Column 2), and covalently bound Tamra cadaverine-labeled nanoparticles (red, Column 3). The images were taken for each system immediately after loading and after 30 min, 72 hr, and 4 weeks of incubation. Scale bars: 60 μm

0.085 (Figure 7). These values indicate that the fabricated scaffolds, despite a high porosity, exhibited gel-like behavior, with the elastic component having a greater influence on the material behavior.

3.2 | Nanoparticle synthesis

The UV-initiated emulsion polymerization scheme allowed for the synthesis of nanoparticles with hydrodynamic radii between 60 and 80 nm (Figure 8). In addition, the particles were relatively monodisperse, with polydispersity indices around 0.170 (Figure 8b). Finally, comparing the properties between batches, the present particle synthesis scheme led to a minimal batch-to-batch variability and provided a reproducible method for the synthesis of P(MMA-co-MAA) particles.

The synthesized particles presented a zeta potential of around -22 mV at physiological pH, indicating that the particles carry a net negative charge and form a stable suspension in these conditions (Figure 9). In increasingly acidic environments, the particle zeta potential increased toward 0 mV with an observed pK_a of 3.50, resulting in a reduction of the net charges and, thus, decreased ability for the repulsion between particles (Figure 9a). This decreased ability for repulsion led to the aggregation of the particles, as pH decreased (Figure 10). While particle sizes remained below 100 nm at pH values above 7, the recorded hydrodynamic diameter progressively increased as pH reduced, reaching values of up to 13 μm (Figure 10a). This increase reflects the formation of micron-scale aggregates as the particle net surface charge decreased. Furthermore, it was shown that

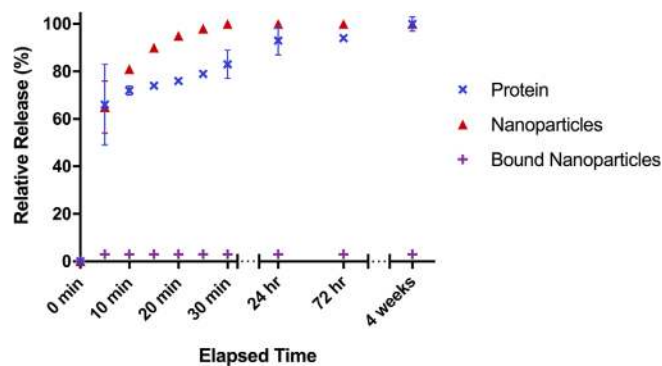


FIGURE 12 The relative cumulative release of DAPI-labeled protein (blue), tamra cadaverine labeled nanoparticles (red), and tamra cadaverine labeled bound nanoparticles (purple) from a chitosan scaffold as a function of time

this aggregation of particles as a result of a decrease in pH was a reversible phenomenon, as the particles regained their original properties when the pH was increased again (Figure 10a,b).

3.3 | Immobilization of nanoparticles within the scaffold

Fluorescent images obtained immediately after loading showed a high fluorescent intensity for all three systems, indicating the presence of protein (in blue) and particles (in red) within the bulk of the scaffolds

(Figure 11). After 30 min of incubation and five washes in phosphate-buffered saline, a significant reduction in the amount of blue was observed, suggesting that within 30 min a large portion of the protein has diffused out of the scaffolds (Figure 11, column 1). Similarly, a reduction in the amount of red was observed for the unbound

particles, but the intensity remained relatively constant for the covalently bound particles (Figure 11, columns 2 and 3). The fluorescent intensity of both the unbound protein and unbound particles continued to decrease over time, with no detectable presence in either system after 4 weeks (Figure 11, row 4). The covalently bound particle

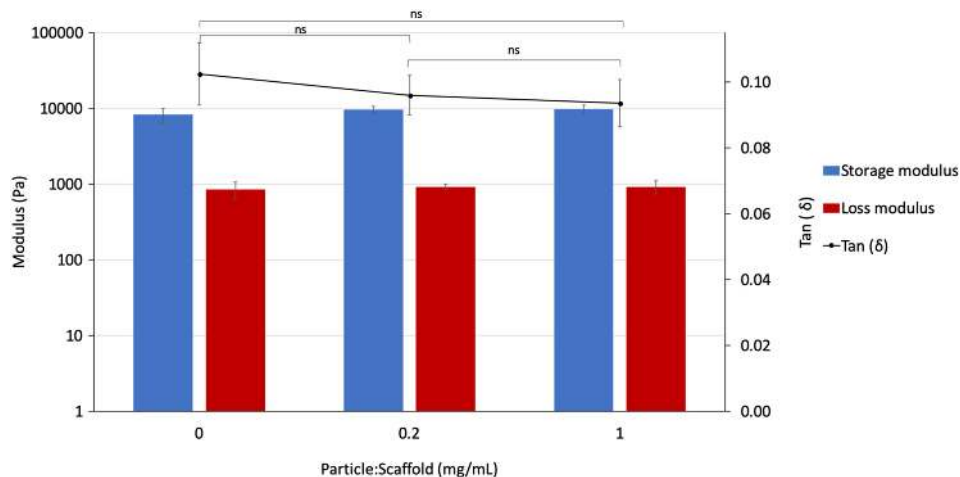


FIGURE 13 The dynamic mechanical properties of two-phase scaffold-nanoparticle system with increasing ratios of particle mass to scaffold volume. ns indicates the difference is not significant

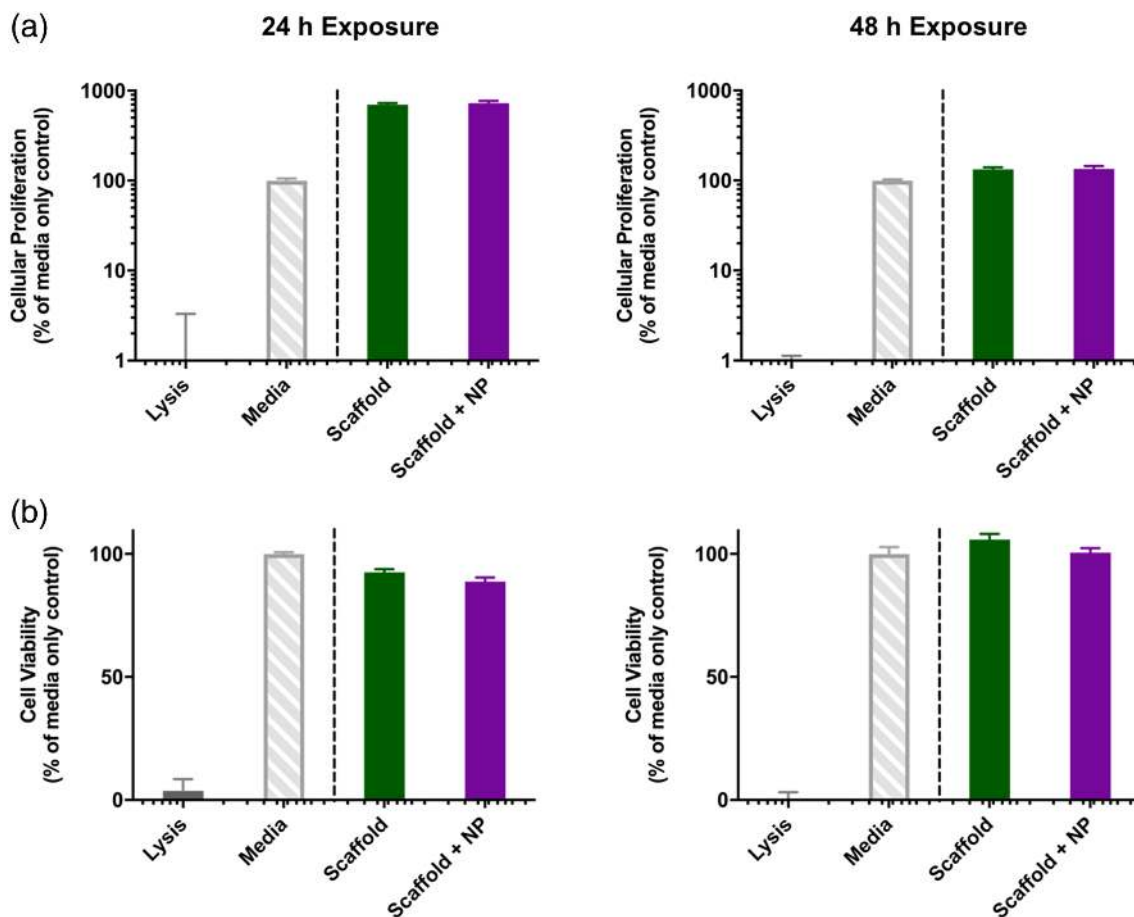


FIGURE 14 The evaluation of the cytocompatibility of 2 wt% chitosan scaffolds with and without bound P(MMA-co-MAA) nanoparticles. (a) Cytocompatibility of HUVEC cells using an MTS cellular proliferation assay after 24 hr (left) and 48 hr exposure (right). (b) Cytocompatibility of HUVEC cells using an LDH cell membrane integrity assay after 24 hr (left) and 48 hr exposure (right)

system, however, continued to show similar intensities across the different time points (Figure 11, column 3).

A quantitative analysis was carried out by plotting the cumulative release as a function of time (Figure 12). A rapid burst release was observed for the adsorbed protein and nanoparticles, with over 60% released within the first 5 min for both systems and 100% release after 4 weeks (Figure 12). An initial burst release of about 3% within the first 5 min was observed for the covalently bound nanoparticles with no further release for up to 4 weeks (Figure 12).

Finally, the incorporation of covalently bound nanoparticles within the scaffold bulk did not have a significant effect on the scaffold mechanical properties (Figure 13). While a slight increase in the storage modulus and a decrease in loss modulus was observed for increasing amounts of nanoparticles within the scaffold, these changes remained within the margins of error (Figure 13).

3.4 | In vitro cytotoxicity studies

The results of cell proliferation and cell viability assays for HUVECs in the presence of 2 wt% chitosan scaffolds with and without covalently bound nanoparticles indicate that the scaffold systems did not have a toxic effect on the cells (Figure 14). After 24 and 48 hr of exposure, both the scaffolds and scaffolds with nanoparticle systems resulted in cell viabilities of above 95% relative to the media control, indicating that the system components did not result in cell lysis after 48 hr (Figure 14b).

Furthermore, after 24 hr of exposure to both the scaffolds and the scaffolds with covalently bound nanoparticles, the cells exhibited relative cellular proliferations of up to 800%, when compared to the media control. This effect, while less significant, is still observed after 48 hr of exposure to the scaffold systems, with proliferation values up to 150% (Figure 14a).

4 | DISCUSSION

4.1 | Chitosan scaffolds for bone tissue engineering applications

The mechanical properties of bone tissue engineering scaffolds are considered to be an essential characteristic to promote the osteogenic behavior of the biomaterial. Typical values of the compressive strength of cancellous bone are between 2 and 12 MPa while elastic moduli range between 0.1 and 5 GPa (Wu, Liu, Yeung, Liu, & Yang, 2014). In addition, the dynamic mechanical properties of cancellous bone have been found to be 800 kPa for the storage modulus, and 52 kPa for the loss modulus (Töyräs, Nieminen, Kröger, & Jurvelin, 2002; Yilgor, Sousa, Reis, Hasirci, & Hasirci, 2008).

Natural polymers are highly attractive materials for bone tissue engineering scaffold applications due to their abundance in nature, inherent chemical biocompatibility, and biodegradability. Chitosan, in particular, presents mucoadhesive and antibacterial properties and has been shown to be osteoconductive (Venkatesan, Anil, Kim, & Shim, 2017). A further

advantage of chitosan in the proposed two-phase system is the presence of reactive primary amines along the polymer backbone, which can be used for the immobilization of nanocarriers with reactive carboxyl groups via carbodiimide-crosslinker chemistry. However, a key limitation in the use of natural polymers in general and chitosan, in particular, are their low mechanical strength, though methods have been developed to fabricate high-strength natural-polymer based scaffold systems. Often these systems rely on the fabrication of natural polymer-based composites in combination with ceramics or synthetic polymers (Rao, Harini, Shad-amarshan, Balagangadharan, & Selvamurugan, 2017). More recently, however, a number of methods have been developed in order to fabricate high-strength pristine natural polymer-based systems (Jana, Florczyk, Leung, & Zhang, 2012).

In this work, scaffolds were fabricated by lyophilization of the chitosan solutions, often referred to in the literature as the “freeze-drying method” (Beck, Jiang, Nair, & Laurencin, 2017). This method forms scaffolds with interconnected, large-scale pores and is, thus, of particular interest for bone tissue engineering. The observed pore size of around 300 μm has been considered optimal for bone tissue engineering applications (Karageorgiou & Kaplan, 2005; Loh & Choong, 2013). In addition, the presence of larger-scale macropores was observed. This range in pore size could present further advantages for the regeneration of bone tissue, as it has been demonstrated that a hierarchical structure with multi-scale porosity can lead to higher osteoconductivity than systems with a uniform pore size (Woodard et al., 2007).

The fabrication of bone tissue engineering scaffolds often leads to a trade-off between interconnected porosity and sufficient mechanical properties, since an increase in porosity and pore size can result in a loss of mechanical integrity. The lyophilization method used in the present work led to the fabrication of scaffolds with a storage modulus of around 8.5 kPa. Wang and Stegemann developed crosslinked chitosan/collagen hydrogels for bone tissue engineering applications with a storage modulus of up to 0.35 kPa (Wang & Stegemann, 2011). Similarly, Jin et al. (2009) developed an injectable chitosan-based scaffold with a storage modulus of up to 0.5 kPa in physiological conditions. Therefore, when comparing the present system to the systems existing in the literature, it is concluded that the freeze-drying system is a promising method to fabricate higher strength hydrated natural polymer networks.

In addition, the SEM images revealed a degree of anisotropy in the fabricated scaffold as a result of pore orientation. This is a desirable property in the design of bone scaffolds, since bone is primarily loaded anisotropically in the body (Fisher & Peppas, 2009). Furthermore, this characteristic is especially desirable for the regeneration of cancellous bone tissue, which itself is an anisotropic material with viscoelastic mechanical behavior (Mathieu et al., 2006).

4.2 | Effect of nanoparticle immobilization on their sustained retention and scaffold properties

The majority of growth factor delivery systems explored in the literature rely on the adsorption of growth factors within the bulk of highly

porous scaffolds (Ferrand et al., 2014; Simmons, Alsborg, Hsiong, Kim, & Mooney, 2004). A key limitation of that approach is a rapid burst release of the incorporated protein. This behavior can be explained by the highly porous nature of the scaffolds used for bone tissue engineering applications, which allows for growth factors with diameters of only several nanometers to easily diffuse through the pore network. However, this leads to a trade-off, since high porosities are considered to be necessary for the design of bone tissue engineering scaffolds and have been found to be essential to the vascularization of the newly forming bone (Annabi et al., 2010; Karageorgiou & Kaplan, 2005; Wu et al., 2014). Furthermore, the likelihood of a burst release profile is increased upon implantation of the scaffold into the body due to the highly dynamic physiological environment where fluid flow and diffusion can limit protein retention.

One common approach for the improved retention of growth factors within the scaffold bulk is through their encapsulation into nanoparticles (Park, Kim, Moon, & Na, 2009; Wang et al., 2015). This method has been shown to lead to improved release profiles, still presenting an initial burst release, which is followed by a sustained release profile. However, the ratio of the particle diameter to the scaffold pore size remains extremely small, with most nanoparticle systems having a diameter of around 100 nm and pore sizes for bone tissue engineering scaffolds ranging between 200 and 500 μm . Nanoparticles can, thus, easily diffuse out of the scaffold once they are implanted in the body and put in contact with dynamic fluid flow *in vivo*.

The system developed in this study aims to eliminate the potential of both protein and particles to diffuse rapidly out of the scaffold bulk through a novel approach: the covalent binding of particles to the scaffold backbone. While covalent binding approaches have previously been used for growth factor delivery applications, the previous systems rely on the covalent binding of the growth factors themselves to the scaffold backbone. However, this method poses concerns due to the negative effects on protein bioactivity (Di Luca et al., 2017).

The results of the fluorescent imaging experiment suggest that the common methods of growth factor and nanoparticle incorporation into scaffolds result in their rapid diffusion out of the scaffold bulk. Proteins in the scaffold were no longer visibly detectable after 72 hr and nanoparticles were fully removed after 4 weeks. In contrast, the nanoparticles that were covalently bound to the scaffold were still present within the scaffold after 4 weeks. These results suggest that the diffusion of nanoparticles out of the scaffold carrier can present a significant limitation to the systems proposed in the literature. Meanwhile, the novel approach of covalently binding nanocarriers to the scaffold bulk can limit diffusion out of the scaffold. Furthermore, the retention of nanoparticles for multiple weeks reflects the potential of such systems to deliver essential growth factors, such as BMP-2 that are desired to be present within bone regeneration sites for up to 4 weeks after injury (Hankenson, Gagne, & Shaughnessy, 2015).

The incorporation of nanoparticles within the scaffold bulk may also provide further advantages, such as improved mechanical properties and structural hierarchy, which can further promote the regeneration of bone tissue (Wang et al., 2015). In the present work, no

significant change in the mechanical properties was detected for the incorporation of 0.2 and 1 mg/ml of covalently bound nanoparticles within the scaffold when compared to the control chitosan scaffold. However, this can be explained by the low concentrations of nanoparticles tested, and systems could be developed that incorporate unloaded nanoparticles as well as loaded nanoparticles to improve the mechanical properties of the scaffolds without affecting the delivered dose of growth factors.

Finally, *in vitro* studies evaluating the effects of chitosan scaffolds with and without covalently bound P(MMA-co-MAA) nanoparticles on the viability and proliferation of HUVEC indicate that the incorporation of nanoparticles within the chitosan scaffolds through covalent binding does not have a cytotoxic effect on HUVECs. In fact, *in vitro* results suggest that the 2 wt% chitosan scaffolds can lead to increased HUVEC proliferation in the first 48 hr of exposure when compared to a media control and that this effect is not reduced by the incorporation of covalently bound nanoparticles. Chitosan has been identified as an excellent pro-angiogenic biomaterial and its use has also been explored in cardiovascular tissue engineering applications (Deng et al., 2010). Indeed, chitosan has been commonly incorporated into collagen-based tissue engineering systems in order to improve vascularization (Ellis & Korbitt, 2017). McBane et al. (2013) have shown that the fabrication of a 10:1 collagen: chitosan hydrogel leads to increased endothelial progenitor cell viability and endothelial differentiation when compared to a pure collagen scaffold. The pro-angiogenic characteristics of chitosan as demonstrated in the literature, therefore, explain the observed increase in HUVEC proliferation on the chitosan scaffolds when compared to the media controls. The cytocompatibility and proliferative effects of the proposed two-phase scaffold-nanoparticle system constitutes a promising approach to promote the regeneration of vascularized bone tissue.

5 | CONCLUSIONS

The present work provides a method and proof-of-concept for the development of a novel two-phase bone tissue engineering system, consisting of a porous chitosan scaffold that incorporates covalently bound nanocarriers for the sustained delivery of osteogenic growth factors.

Highly porous chitosan scaffolds were fabricated according to a lyophilization method. This simple technique allows for the fabrication of relatively high-strength scaffolds when compared to other available natural polymer-based scaffolds, as well as an interconnected pore network with varying pore diameters and anisotropic structure.

To further improve on the systems existing in the literature, carbodiimide-crosslinker chemistry was used to bind P(MMA-co-MAA) nanoparticles to the chitosan backbone. The results of this work demonstrate that this novel approach eliminates the risk of nanoparticle diffusion out of the scaffold bulk. In particular, nanoparticles were retained over the relevant therapeutic timeframe for bone regeneration.

Ultimately, this approach has the potential to be extended beyond bone regeneration, to any tissue for which growth factor

retention poses a risk to proper tissue growth. Indeed, the mechanical properties and even polymer selection can be modulated to suit the specific needs of other target tissues. Furthermore, nanoparticles with controllable degradation rates can be used to further improve the tunability of such systems.

ACKNOWLEDGMENTS

This work was supported by the National Institutes of Health Grant R01-EB022025 and the UT-Portugal Collaborative Research Program (CoLAB) "Intelligent Scaffolds for Molecular Recognition of Advanced Applications in Regenerative Medicine". We acknowledge helpful technical discussions with Drs. Julia Vela Ramirez and John R. Clegg.

ORCID

Tinke-Marie De Witte  <https://orcid.org/0000-0001-9469-1946>

REFERENCES

- Amini, A. R., Laurencin, C. T., & Nukavarapu, S. P. (2012). Bone tissue engineering: Recent advances and challenges. *Critical Reviews in Biomedical Engineering*, 40, 363–408.
- Annabi, N., Nichol, J. W., Zhong, X., Ji, C., Koshy, S., Khademhosseini, A., & Dehghani, F. (2010). Controlling the porosity and microarchitecture of hydrogels for tissue engineering. *Tissue Engineering. Part B, Reviews*, 16, 371–383.
- Balagangadharan, K., Dhivya, S., & Selvamurugan, N. (2017). Chitosan based nanofibers in bone tissue engineering. *International Journal of Biological Macromolecules*, 104, 1372–1382.
- Beck, S. C., Jiang, T., Nair, L. S., & Laurencin, C. T. (2017). Chitosan for bone and cartilage regenerative engineering. In J. A. Jennings & J. D. Bumgardner (Eds.), *Chitosan based biomaterials* (Vol. 2, pp. 33–72). Sawston: Woodhead Publishing.
- Bessa, P. C., Machado, R., Nürnberger, S., Dopler, D., Banerjee, A., Cunha, A. M., ... Casal, M. (2010). Thermoresponsive self-assembled elastin-based nanoparticles for delivery of BMPs. *Journal of Controlled Release*, 142, 312–318.
- Bose, S., Roy, M., & Bandyopadhyay, A. (2012). Recent advances in bone tissue engineering scaffolds. *Trends in Biotechnology*, 30, 546–554.
- Calori, G. M., Colombo, M., Mazza, E. L., Mazzola, S., Malagoli, E., & Mineo, G. V. (2014). Incidence of donor site morbidity following harvesting from the iliac crest or RIA graft. *Injury*, 45(Suppl 6), S116–S120.
- Chen, D., Zhao, M., & Mundy, G. R. (2004). Bone morphogenetic proteins. *Growth Factors*, 22, 233–241.
- De Witte, T.-M., Fratila-Apachitei, L. E., Zadpoor, A. A., & Peppas, N. A. (2018). Bone tissue engineering via growth factor delivery: From scaffolds to complex matrices. *Regenerative Biomaterials*, 5, 197–211.
- Deng, C., Zhang, P., Vulesevic, B., Kuraitis, D., Li, F., Yang, A. F., ... Suuronen, E. J. (2010). A collagen–chitosan hydrogel for endothelial differentiation and angiogenesis. *Tissue Engineering. Part A*, 16, 3099–3109.
- Di Luca, A., Klein-Gunnewiek, M., Vancso, J. G., van Blitterswijk, C. A., Benetti, E. M., & Moroni, L. (2017). Covalent binding of bone morphogenetic Protein-2 and transforming growth factor- β 3 to 3D plotted scaffolds for osteochondral tissue regeneration. *Biotechnology Journal*, 12, 1700268. <https://doi.org/10.1002/biot.201700072>
- Dimitriou, R., Mataliotakis, G. I., Angoules, A. G., Kanakaris, N. K., & Giannoudis, P. V. (2011). Complications following autologous bone graft harvesting from the iliac crest and using the RIA: A systematic review. *Injury*, 42(Suppl 2), S3–S15.
- El Bialy, I., Jiskoot, W., & Reza Nejadnik, M. (2017). Formulation, delivery and stability of bone morphogenetic proteins for effective bone regeneration. *Pharmaceutical Research*, 34, 1152–1170.
- Ellis, C. E., & Korbitt, G. S. (2017). Chitosan-based biomaterials for treatment of diabetes. In J. A. Jennings & J. D. Bumgardner (Eds.), *Chitosan based biomaterials* (Vol. 2, pp. 91–113). Sawston: Woodhead Publishing.
- Ferrand, A., Eap, S., Richert, L., Lemoine, S., Kalaskar, D., Demoustier-Champagne, S., ... Benkirane-Jessel, N. (2014). Osteogenetic properties of electrospun Nanofibrous PCL scaffolds equipped with chitosan-based Nanoreservoirs of growth factors. *Macromolecular Bioscience*, 14, 45–55.
- Fisher, O. Z., & Peppas, N. A. (2009). Polybasic Nanomatrices prepared by UV-initiated Photopolymerization. *Macromolecules*, 42, 3391–3398.
- Fröhlich, M., Grayson, W. L., Wan, L. Q., Marolt, D., Drobnic, M., & Vunjak-Novakovic, G. (2008). Tissue engineered bone grafts: Biological requirements, tissue culture and clinical relevance. *Current Stem Cell Research & Therapy*, 3, 254–264.
- Habibovic, P. (2017). Strategic directions in Osteoinduction and biomimetics. *Tissue Engineering Part A*, 23, 1295–1296.
- Hankenson, K. D., Gagne, K., & Shaughnessy, M. (2015). Extracellular signaling molecules to promote fracture healing and bone regeneration. *Advanced Drug Delivery Reviews*, 94, 3–12.
- Jana, S., Florczyk, S. J., Leung, M., & Zhang, M. (2012). High-strength pristine porous chitosan scaffolds for tissue engineering. *Journal of Materials Chemistry*, 22, 6291–6299.
- Jin, R., Moreira Teixeira, L. S., Dijkstra, P. J., Karperien, M., van Blitterswijk, C. A., Zhong, Z. Y., & Feijen, J. (2009). Injectable chitosan-based hydrogels for cartilage tissue engineering. *Biomaterials*, 30, 2544–2551.
- Karageorgiou, V., & Kaplan, D. (2005). Porosity of 3D biomaterial scaffolds and osteogenesis. *Biomaterials*, 26, 5474–5491.
- Loh, Q. L., & Choong, C. (2013). Three-dimensional scaffolds for tissue engineering applications: Role of porosity and pore size. *Tissue Engineering Part B: Reviews*, 19, 485–502.
- Mathieu, L. M., Mueller, T. L., Bourban, P.-E., Pioletti, D. P., Müller, R., & Månson, J. A. (2006). Architecture and properties of anisotropic polymer composite scaffolds for bone tissue engineering. *Biomaterials*, 27, 905–916.
- McBane, J. E., Vulesevic, B., Padavan, D. T., McEwan, K. A., Korbitt, G. S., & Suuronen, E. J. (2013). Evaluation of a collagen–chitosan hydrogel for potential use as a pro-angiogenic site for islet transplantation. *PLoS One*, 8, e77538.
- Myeroff, C., & Archdeacon, M. (2011). Autogenous bone graft: donor sites and techniques. *The Journal of Bone and Joint Surgery. American Volume*, 93, 2227–2236.
- Oryan, A., Alidadi, S., Moshiri, A., & Maffulli, N. (2014). Bone regenerative medicine: Classic options, novel strategies, and future directions. *Journal of Orthopaedic Surgery and Research*, 9, 18.
- Park, K.-H., Kim, H., Moon, S., & Na, K. (2009). Bone morphogenetic protein-2 (BMP-2) loaded nanoparticles mixed with human mesenchymal stem cell in fibrin hydrogel for bone tissue engineering. *Journal of Bioscience and Bioengineering*, 108, 530–537.
- Rao, S. H., Harini, B., Shadamarshan, R. P. K., Balagangadharan, K., & Selvamurugan, N. (2017). Natural and synthetic polymers/bioceramics/bioactive compounds-mediated cell signaling in bone tissue engineering. *International Journal of Biological Macromolecules*, 110, 88–96. <https://doi.org/10.1016/j.ijbiomac.2017.09.029>
- Saravanan, S., Leena, R. S., & Selvamurugan, N. (2016). Chitosan based bio-composite scaffolds for bone tissue engineering. *International Journal of Biological Macromolecules*, 93, 1354–1365.
- Simmons, C. A., Alsberg, E., Hsiong, S., Kim, W. J., & Mooney, D. J. (2004). Dual growth factor delivery and controlled scaffold degradation enhance in vivo bone formation by transplanted bone marrow stromal cells. *Bone*, 35, 562–569.
- Subbiah, R., Hwang, M. P., Van, S. Y., Do, S. H., Park, H., Lee, K., ... Park, K. (2015). Osteogenic/Angiogenic dual growth factor delivery

- microcapsules for regeneration of vascularized bone tissue. *Advanced Healthcare Materials*, 4, 1982–1992.
- Töyräs, J., Nieminen, M. T., Kröger, H., & Jurvelin, J. S. (2002). Bone mineral density, ultrasound velocity, and broadband attenuation predict mechanical properties of trabecular bone differently. *Bone*, 31, 503–507.
- Venkatesan, J., Anil, S., Kim, S.-K., & Shim, M. S. (2017). Chitosan as a vehicle for growth factor delivery: Various preparations and their applications in bone tissue regeneration. *International Journal of Biological Macromolecules*, 104, 1383–1397.
- Vo, T. N., Kasper, F. K., & Mikos, A. G. (2012). Strategies for controlled delivery of growth factors and cells for bone regeneration. *Advanced Drug Delivery Reviews*, 64, 1292–1309.
- Wang, L., & Stegemann, J. P. (2011). Glyoxal crosslinking of cell-seeded chitosan/collagen hydrogels for bone regeneration. *Acta Biomaterialia*, 7, 2410–2417.
- Wang, Z., Wang, K., Lu, X., Li, M., Liu, H., Xie, C., ... Zhi, W. (2015). BMP-2 encapsulated polysaccharide nanoparticle modified biphasic calcium phosphate scaffolds for bone tissue regeneration. *Journal of Biomedical Materials Research*, 103, 1520–1532.
- Woodard, J. R., Hilldore, A. J., Lan, S. K., Park, C. J., Morgan, A. W., Eurell, J. A. C., ... Wagoner Johnson, A. J. (2007). The mechanical properties and osteoconductivity of hydroxyapatite bone scaffolds with multi-scale porosity. *Biomaterials*, 28, 45–54.
- Wu, S., Liu, X., Yeung, K. W. K., Liu, C., & Yang, X. (2014). Biomimetic porous scaffolds for bone tissue engineering. *Materials Science & Engineering R: Reports*, 80, 1–36.
- Yilgor, P., Sousa, R. A., Reis, R. L., Hasirci, N., & Hasirci, V. (2008). 3D plotted PCL scaffolds for stem cell based bone tissue engineering. *Macromolecular Symposia*, 269, 92–99.

How to cite this article: De Witte T-M, Wagner AM, Fratila-Apachitei LE, Zadpoor AA, Peppas NA. Immobilization of nanocarriers within a porous chitosan scaffold for the sustained delivery of growth factors in bone tissue engineering applications. *J Biomed Mater Res*. 2020;108A: 1122–1135. <https://doi.org/10.1002/jbm.a.36887>